ISTITUTO NAZIONALE DI FISICA NUCLEARE

Sezione di Pisa

INFN/TC-82/1
10 Febbraio 1982

R. Bellazzini, A. Del Guerra, M. M. Massai, M. Ragadini, G. Spandre and G. Tonelli:

DIGITAL AUTORADIOGRAPHY OF HUMAN LIVING CELLS WITH A MWPC.

Servizio Documentazione
dei Laboratori Nazionali di Frascati

Istituto Nazionale di Fisica Nucleare
Sezione di Pisa

INFN/TC-82/1
10 Febbraio 1982

DIGITAL AUTORADIOGRAPHY OF HUMAN LIVING CELLS WITH A MWPC

R. Bellazzini, A. Del Guerra, M. M. Massai, M. Ragadini, G. Spandre and G. Tonelli
Istituto di Fisica dell'Università - P. zza Torricelli, 2 - 56100 Pisa (Italy), and
INFN, Sezione di Pisa - Via Livornese - 56010 San Piero a Grado (Italy)

ABSTRACT

The possibility of using a MWPC for the non-destructive identification of DNA repair deficient mammalian cells is discussed.

The detection system relies on mapping the differential incorporation of a radioactive precursor of DNA biosynthesis by aggregates of cells. The resolving power, sensitivity and linearity of the developed system are shown together with preliminary analogically and digitally reconstructed maps of ^{14}C or ^{3}H labelled cells.

1. - INTRODUCTION.

Defects in DNA repair mechanisms are associated with and are probably the cause of some human diseases, but our knowledge of the repair mechanism in mammalian cells is strongly limited by the lack of a suitable method for identification of DNA repair deficient mutant cells. Most of the known repair mechanisms involve the unscheduled synthesis[1] of short DNA sequences which replace the damaged regions. As a consequence, repair deficient mutants may be recognized by their inability to incorporate a radioactive precursor in DNA chains in conditions under which repair should normally occur. DNA damage can be induced by ultraviolet light exposure and a differential incorporation of the labelling agent can be produced with particular procedures, which include a bath of the damaged cells in ^{14}C or ^{3}H-thymidine. As a result, repair-competent cells will incorporate the radioactivity, whereas repair-deficient mutants will stay poorly

labelled. We are then left with the problem of distinguishing rare, poorly labelled colonies interspersed with a great majority of labelled colonies.

Conventional autoradiographic techniques do not meet the particular requirements of this type of study: a) low time consumption, b) high sensitivity, c) need for a non destructive technique to keep the identified biological mutants alive for further biological studies. In previous papers[2, 3] we have shown that a MWPC was able to satisfy these requirements and could be used as an electronic autoradiography system. Here we present the results obtained with a "ad hoc" designed MWPC with optimized mechanical characteristics for the reconstruction of low level β^- activity maps. Test performed with γ and β^- sources are discussed together with electronically reconstructed absorption and transmission images; finally, actual maps of ^{14}C or ^{3}H labelled colonies of living cells are presented.

2. - THE MWPC AND THE ANALOG READ-OUT SYSTEM.

A crucial problem in localizing and identifying small, individual spots of β^- activity with gaseous detectors is connected with the range of the β^--rays inside the detector volume.

The spread-out of an isotropically β^- emitting source at a distance L from the detection plane and with extended (track) ionization can be approximately modelled, assuming rectilinear tracks and exponential attenuation, and neglecting the self-absorption in the source, by

$$\varrho(r) = \frac{N_o}{2\pi}\left[\frac{1}{\lambda}\int_{L-L_o}^{L} \frac{e^{-\frac{\sqrt{r^2+z^2}(2z-L^*)}{z\lambda}}}{r^2+z^2}\,dz + \frac{1}{2L^2}\,\frac{e^{-\frac{L_T\sqrt{1+\frac{r^2}{L^2}}}{\lambda}}}{(1+\frac{r^2}{L^2})^{3/2}}\right] \qquad (1)$$

where N_o is the number of emitted particles, λ the absorption coefficient, L_o the cathode-anode distance, L_T the total absorption thickness (mylar window + gas) and $L^* = 2L - L_T$ (Fig. 1). This equation gives the bidimensional density distribution of the center of gravity of the ionization clouds as a function of the distance from the source projected on the detection plane.

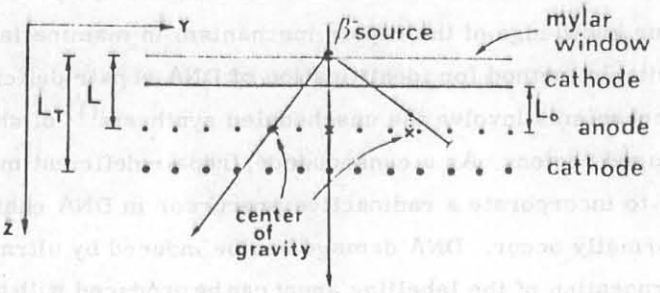

FIG. 1 - Schematic drawing of the MWPC and of the source image spread-out.

The first part of eq. (1) accounts for β^- particles ($\gtrsim 30\%$ of total for ^{14}C) anding their ionization path inside the active volume of the detector, while the second one accounts for particles ending outside.

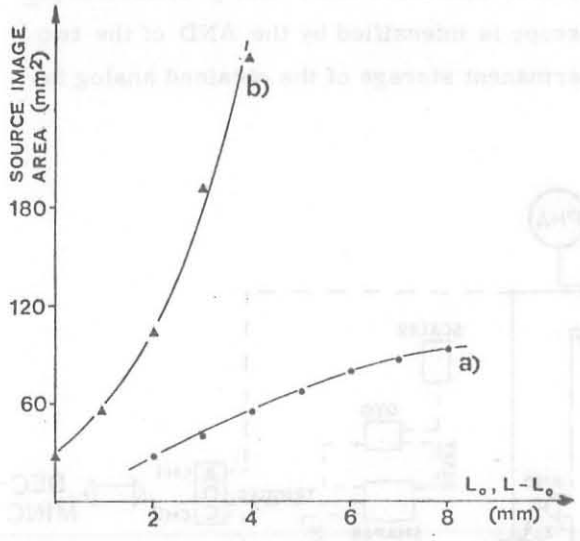

FIG. 2 - The area of the source image as a function of: a) gap-width (L_o) at $L - L_o = 1$ mm; b) source-cathode distance ($L - L_o$) at $L_o = 4$ mm.

The area of the source image, i.e. the area on which 50% of detected events are collected, is shown in Fig. 2 as a function of the main MWPC design parameters.

For improving both resolving power and sensitivity of the detection system to ^{14}C labelled cells we have designed a MWPC with a very thin mylar window (9 μm), small anode-cathode gap (4 mm), and a minimized non-active volume (1 mm: the distance between the cathode plane and the mylar window).

With this design one can obtain a transmission factor of about 70% for the β^- spectrum from ^{14}C, a significant reduction in the spatial extension of the source image and a reasonable compromise with the requirement of detector mechanical and electrostatic stability. Separation between adiacent wires is 2 mm and the total useful detection area is about 600 cm^2. To keep the cost of the associated electronic circuitry reasonably low we have chosen a cathode-coupled delay line read-out system with the anode signal only used as an ENABLE. The delay line and its characteristics has been fully described elsewhere[2]. The one-end start, the other-end stop technique has definite advantages with respect to the anode-start, one-end stop technique in improving the spatial resolution (doubling the relative delay on the two signals and thus doubling the specific delay per unit length), the linearity and the response uniformity (due to compensation effects along the delay line). The pick-up and processing of the signals are obtained by means of low-noise, charge sensitive pre-amplifiers which realize the "cold" termination of the delay-line. The differential and integral shaping constants of the subsequent Timing Filter Amplifiers (TFA ORTEC 454) are selected to optimize the signal-to-noise ratio (Fig. 3). An accurate timing system based

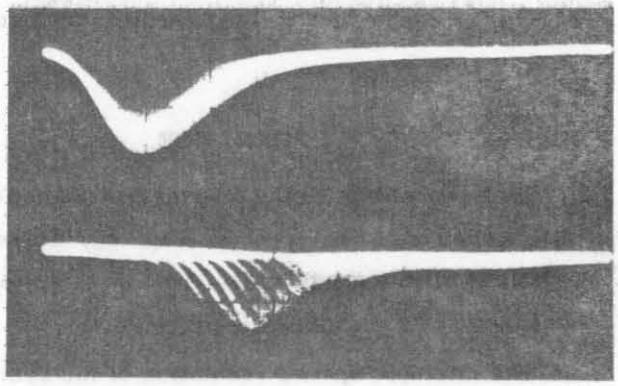

FIG. 3 - One-end delay-line output signals (lower) triggered by the signal from the other end of the delay-line (upper). Horizontal scale is 100 ns/div.

on Constant Fraction Discrimination (CFD ORTEC 583) is used to measure the time of arrival of signals at both ends of the delay-line with accuracy better than 2 ns.

The processed signals from the two ends of each delay-line are the start and stop of two Time to Amplitude Converters (TAC ORTEC 467) that drive the x and y deflection plates of an oscilloscope; the z axis of the oscilloscope is intensified by the AND of the two TAC signals. A Polaroid camera is used as a permanent storage of the obtained analog information (Fig. 4).

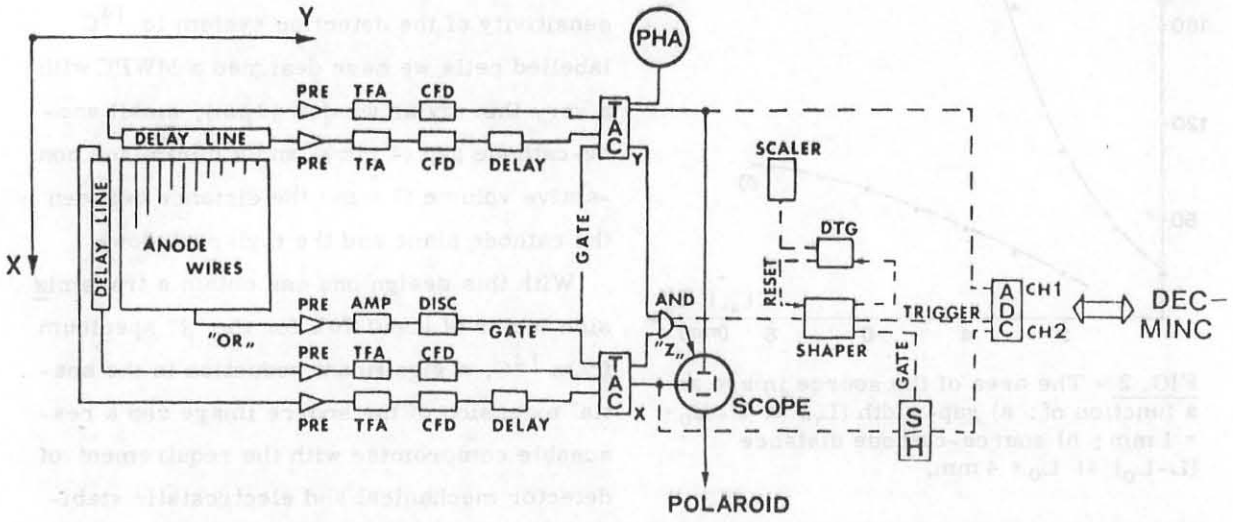

FIG. 4 - Schematic drawing of the electronics and of the read-out system: analog (——) and digital (----) read-out. DTG = dead time generator, S/H = sample and hold unit.

The main limits of this read-out schema are the narrow range of linearity of the Polaroid film and its poor grey level characteristics as well as the impossibility of an off-line analysis. In the next two sections we will discuss the results obtained with this simple and economical read-out system, while in the following sections we will discuss the digital read-out system, its relative advantages and the results obtained with that more complex read-out.

3. - THE MWPC PERFORMANCE.

We have measured the energy resolution for a single anode wire ($\simeq$ 14% FWHM) using a ^{55}Fe source (5.9 KeV X-rays) (Fig. 5a). The energy resolution naturally gets worse ($\simeq$ 30 % FWHM) if all the anode wires are connected together, because of mechanical tolerances and increased system capacity (Fig. 5b).

The intrinsic spatial resolution of the system has been measured irradiating the chamber with an uncollimated ^{55}Fe source and measuring only the coordinate orthogonal to the anode wires. In this configuration the source may be considered as localized within a narrow spot around the sense wire so that the problems related to the finite dimensions of the sour-

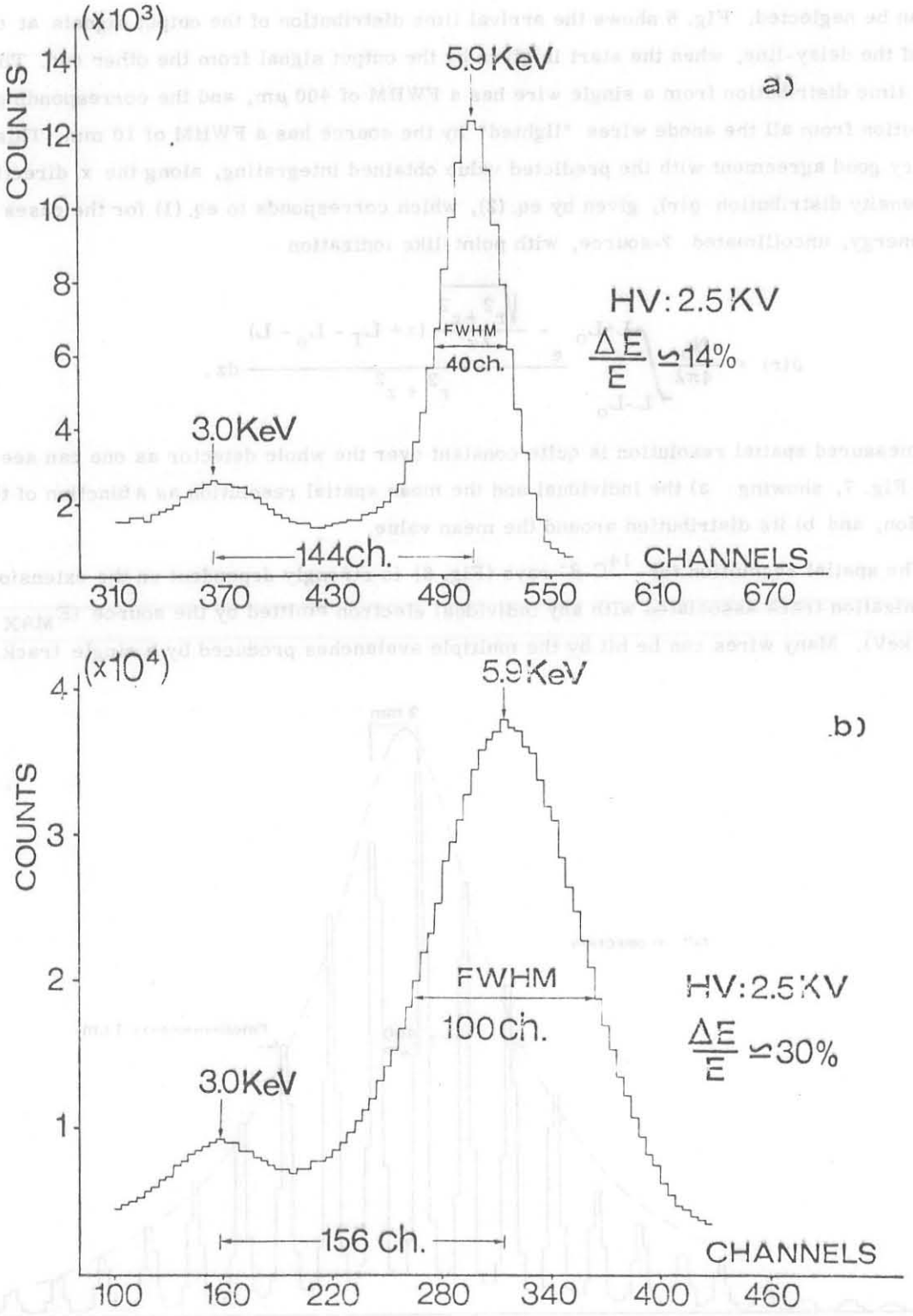

FIG. 5 - Energy resolution spectrum with ^{55}Fe X-rays at the voltage of 2.5 KV: a) single anode wire, b) OR of all the anode wires.

ce can be neglected. Fig. 6 shows the arrival time distribution of the output signals at one end of the delay-line, when the start is given by the output signal from the other end. The arrival time distribution from a single wire has a FWHM of 400 μm, and the corresponding distribution from all the anode wires "lighted" by the source has a FWHM of 10 mm. This is in very good agreement with the predicted value obtained integrating, along the x direction, the density distribution $\varrho(r)$, given by eq. (2), which corresponds to eq. (1) for the cases of low energy, uncollimated γ-source, with point-like ionization

$$\varrho(r) = \frac{N_o}{4\pi\lambda} \int_{L-L_o}^{L+L_o} \frac{e^{-\frac{\sqrt{r^2+z^2}}{\lambda z}(z + L_T - L_o - L)}}{r^2 + z^2} dz . \qquad (2)$$

The measured spatial resolution is quite constant over the whole detector as one can see from Fig. 7, showing: a) the individual and the mean spatial resolution as a function of the position, and b) its distribution around the mean value.

The spatial resolution for ^{14}C β^- rays (Fig. 8) is strongly dependent on the extension of the ionization track associated with any individual electron emitted by the source (E_{MAX} = = 156 keV). Many wires can be hit by the multiple avalanches produced by a single track.

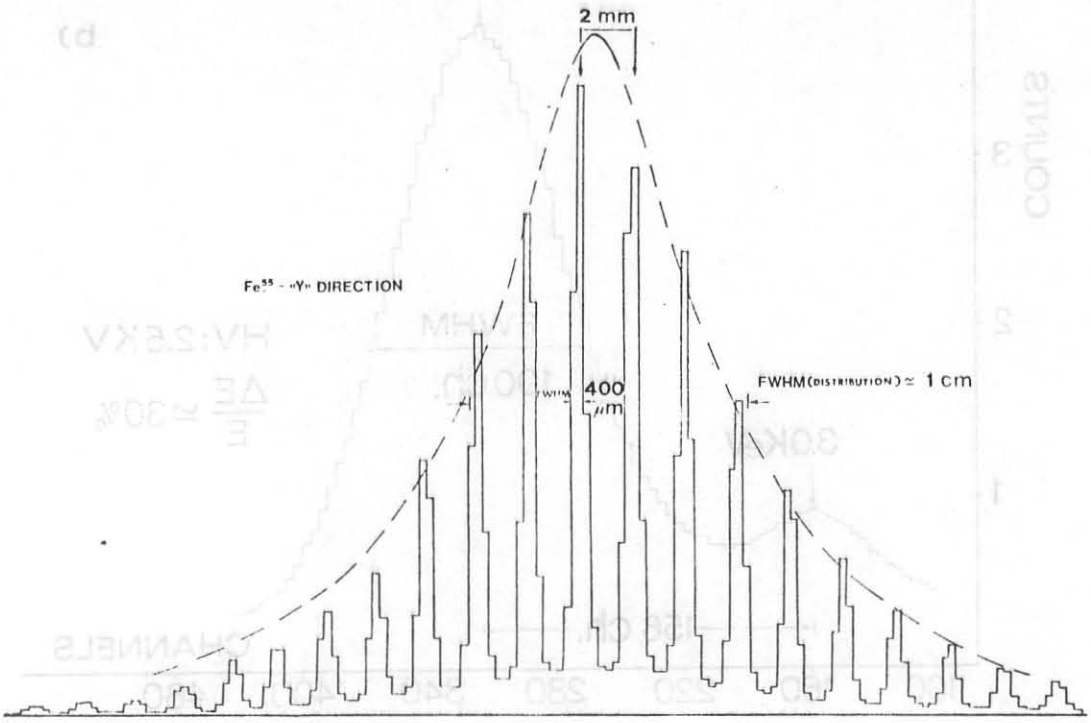

FIG. 6 - Intrinsic spatial resolution as measured with a ^{55}Fe source: —— measured discretized distribution, --- calculated continuous distribution (see also text).

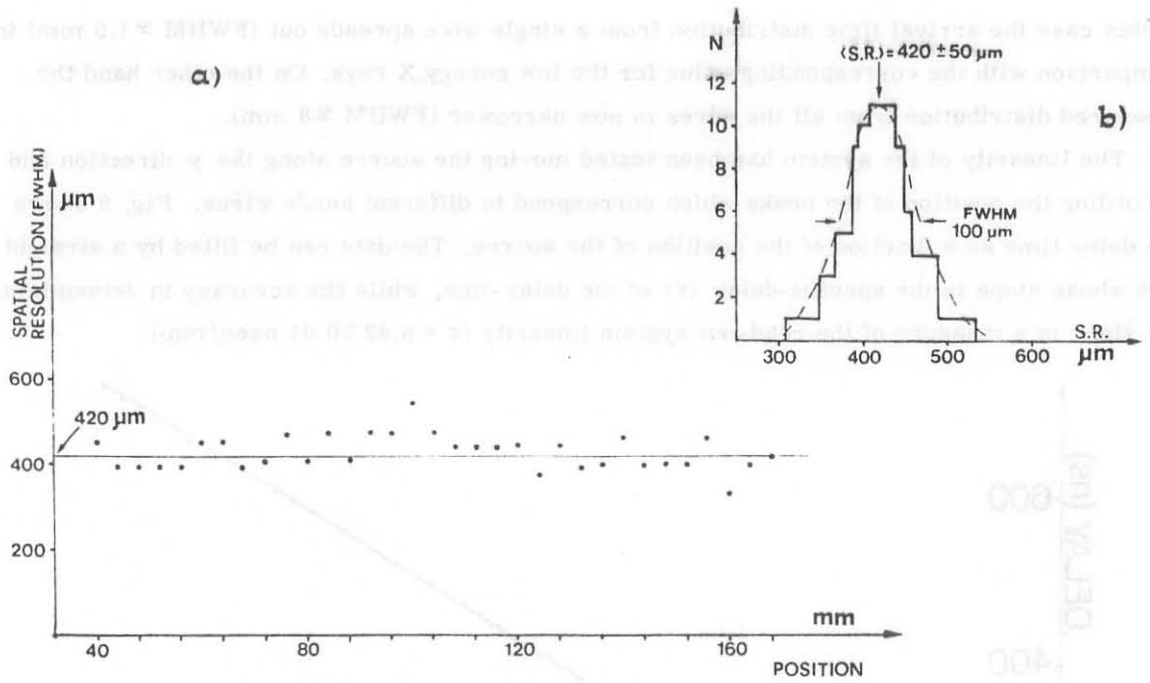

FIG. 7 - a) individual and mean spatial resolution as a function of the distance along the delay-line, b) the dispersion of the measured values.

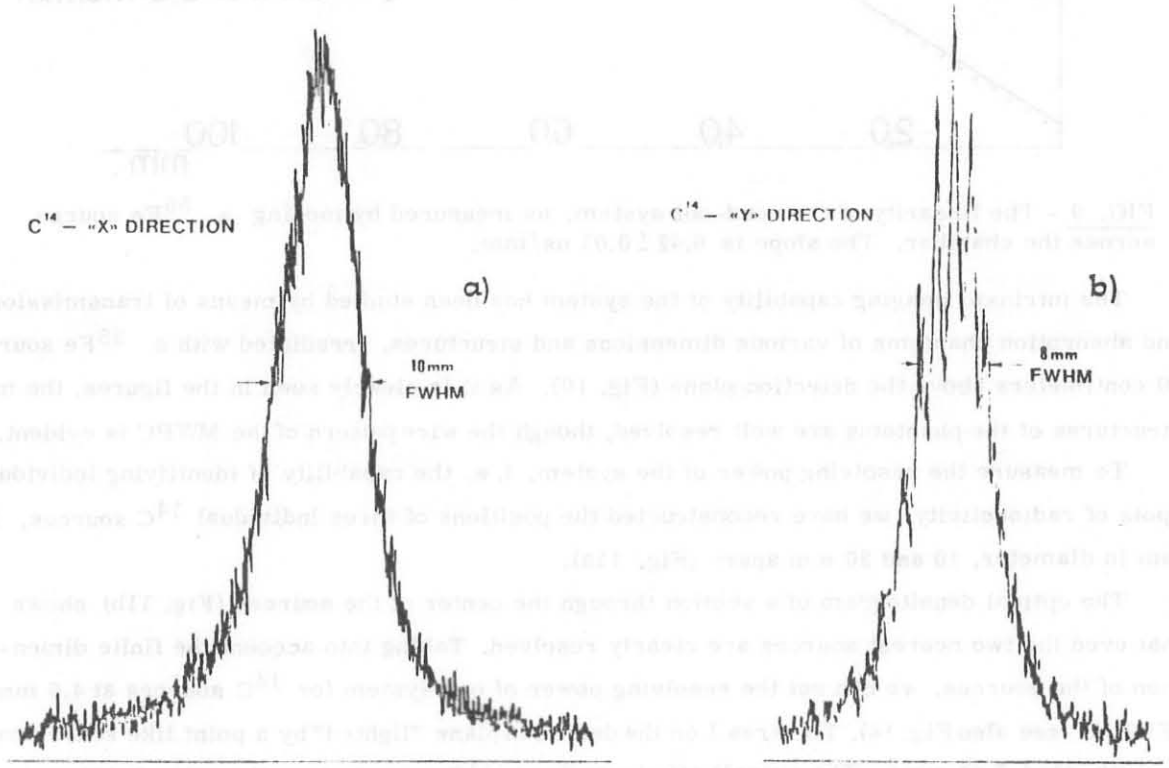

FIG. 8 - Spatial resolution with β^- rays (^{14}C) : a) x-coordinate, b) y-coordinate.

In this case the arrival time distribution from a single wire spreads out (FWHM $\simeq$ 1.5 mm) in comparison with the corresponding value for the low energy X rays. On the other hand the measured distribution from all the wires is now narrower (FWHM $\simeq$ 8 mm).

The linearity of the system has been tested moving the source along the y direction and recording the position of the peaks which correspond to different anode wires. Fig. 9 shows the delay time as a function of the position of the source. The data can be fitted by a straight line whose slope is the specific delay (τ) of the delay-line, while the accuracy in determining the slope is a measure of the read-out system linearity (τ = 6.42 $\pm$ 0.01 nsec/mm).

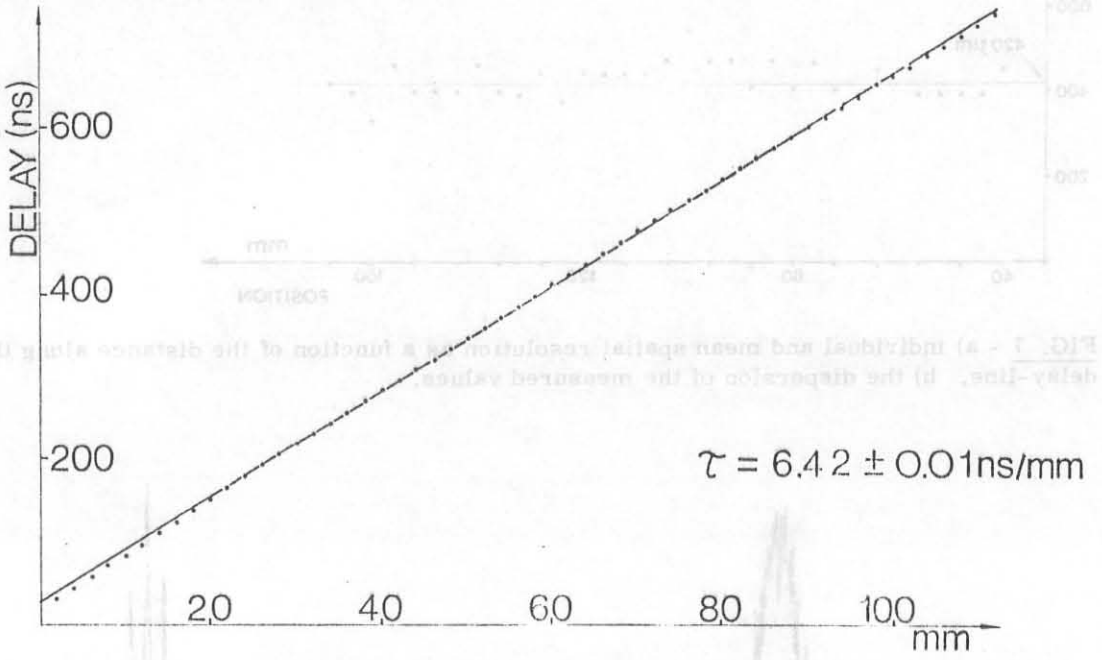

FIG. 9 - The linearity of the read-out system, as measured by moving a ^{55}Fe source across the chamber. The slope is 6.42 $\pm$ 0.01 ns/mm.

The intrinsic imaging capability of the system has been studied by means of transmission and absorption phantoms of various dimensions and structures, irradiated with a ^{55}Fe source 30 centimeters above the detection plane (Fig. 10). As it is clearly seen in the figures, the main structures of the phantoms are well resolved, though the wire pattern of the MWPC is evident.

To measure the resolving power of the system, i.e. the capability of identifying individual spots of radioactivity, we have reconstructed the positions of three individual ^{14}C sources, 2 mm in diameter, 10 and 20 mm apart (Fig. 11a).

The optical densitogram of a section through the center of the sources (Fig. 11b) shows that even the two nearest sources are clearly resolved. Taking into account the finite dimension of the sources, we can set the resolving power of our system for ^{14}C sources at 4.5 mm (FWHM) (see also Fig. 16). The area I on the detection plane "lighted" by a point like source can be estimated $\simeq$ 60 mm^2. The overall efficiency for a ^{14}C source, i.e. the ratio k between the number of β^- particles detected by the chamber and the number of those emitted by the

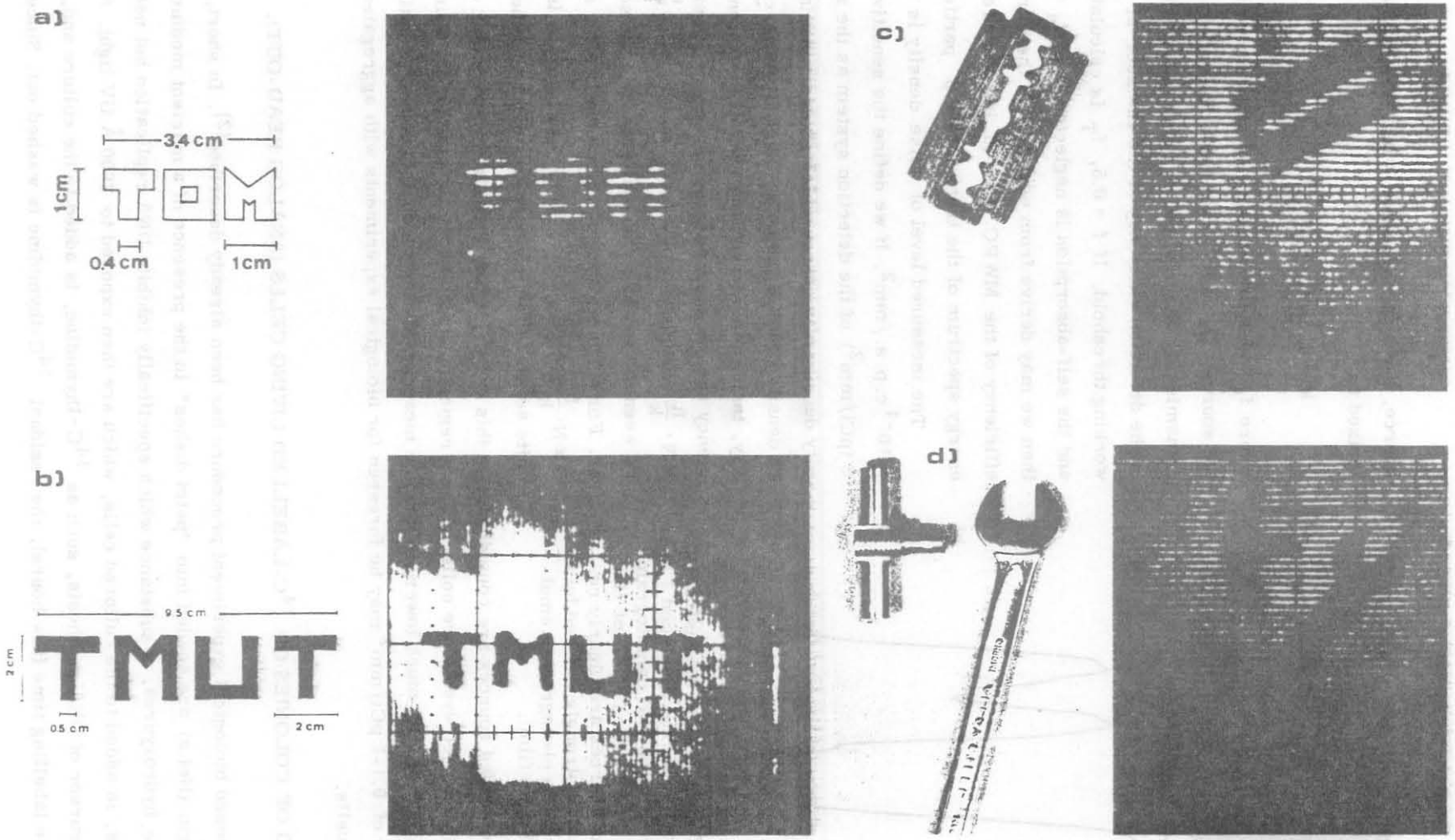

FIG. 10 - Typical images obtained by irradiating various phantoms with a point-like ^{55}Fe source, to illustrate: a) transmission; b), c) and d) absorption phantoms.

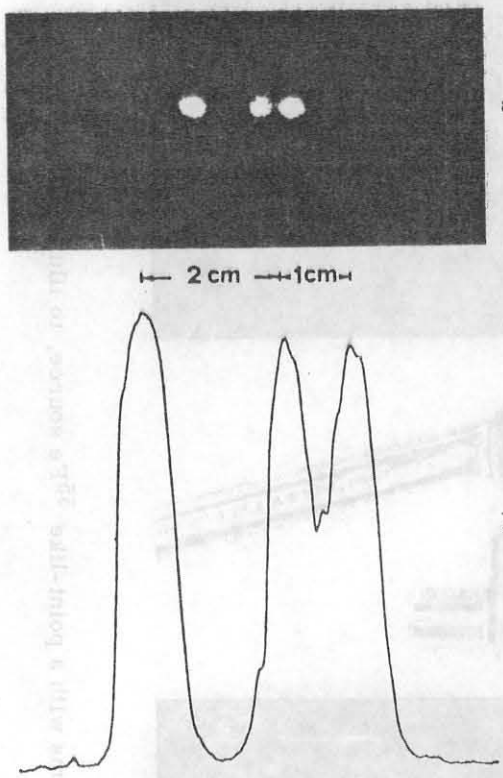

FIG. 11 - a) Analogically reconstructed map of three ^{14}C source displaced 1 and 2 centimeters; b) optical densitogram of a section through the center of the sources. The sources are clearly resolved, although strongly masked by saturation effects in photographic emulsion (the Polaroid film).

source, has been measured $\simeq 0.2$, and can be factorized as:

$$k = f_s f_\Omega f_T \eta_{MWPC} \qquad (2)$$

where f_s takes into account the self-absorption of the source, f_Ω is the solid angle factor, f_T is the transmission factor of the β^- spectrum and η_{MWPC} is the detection efficiency of the chamber at the working threshold. If $f = 0.5$, f_T is calculated 0.7 and the self-absorption is neglected (i.e. $f_s = 1$), then we may derive from equation (2) the intrinsic efficiency of the MWPC $\eta \simeq 0.6$, integrated over the energy spectrum of the transmitted β^- particles.

The measured level of noise density is $N \simeq 10^{-4}$ c.p.s./mm^2. If we define the sensitivity S (pCi/mm^2) of the detection system as the activity density of a source which gives a counting rate density equal to the noise level, then we can say, taking into account the overall detection efficiency and the source image spread-out, that $S \simeq N \cdot \frac{R}{k}$ where $R \sim \frac{A + I + 2(AI)^{1/2}}{A}$ is the ratio between the image and actual area A of the source. For a 1 mm^2 source, numerically $R \simeq I$ and $S \simeq N \cdot \frac{I}{k} \simeq 1$ pCi/mm^2. This result, which is quite adequate for our purposes can be further improved if extended sources are considered. In this case, indeed, R tends toward one, i.e. almost all the detected events are collected on a region not much wider than the actual source area. An activity density much lower can then be measured for extended source configuration. A sensitivity of 0.1-1 pCi/mm^2 may be foreseen for biological experiments with aggregates of mammalian cells.

4. - IMAGING OF COLONIES OF ^{14}C-LABELLED LIVING CELLS (ANALOG READ-OUT).

The proposed biological experiment procedure has been already described[2]. In short, cells of human origin (HeLa) are seeded into "petri dishes" in the presence of a nutrient medium. At a certain time, hydroxyurea, a substance which specifically inhibits DNA replication but not repair synthesis, is added to the cultured cells, which are then exposed to 2600 Å UV light. A radioactive precursor of DNA synthesis, such as ^{14}C-thymidine, is added to the culture and, after an appropriate labelling time (few hours), the residual ^{14}C-thymidine is washed out. Since DNA

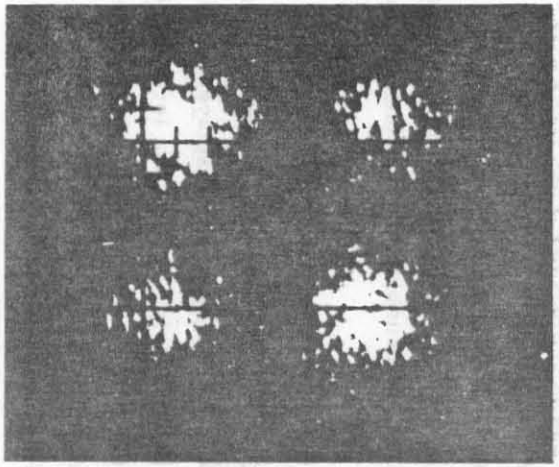

FIG. 12 - Reconstructed map of four cells aggregates, each 2 cm apart and - 10 pCi/mm^2 specific activity.

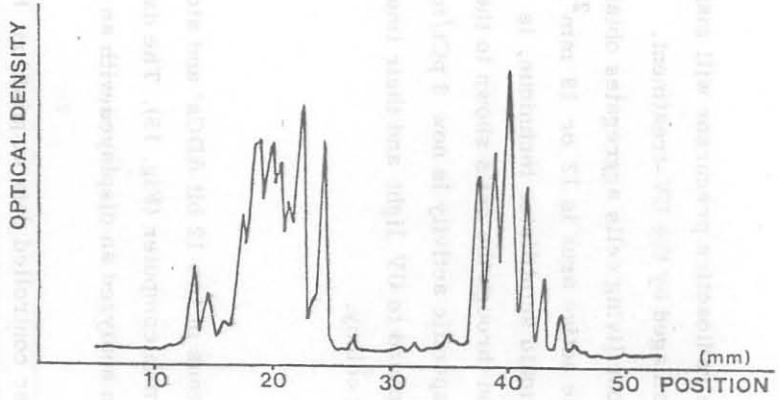

FIG. 13 - Optical densitogram of a section through the cells on the right-hand side of the picture of Fig. 11.

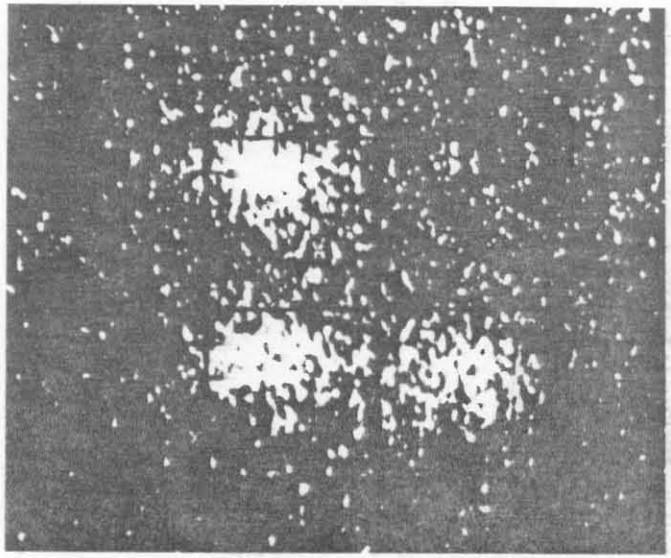

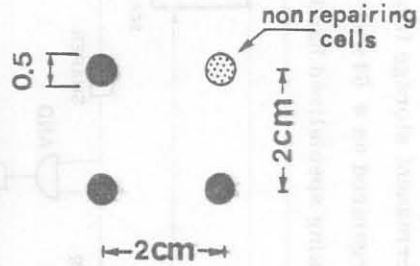

FIG. 14 - Reconstructed map of three cells aggregates, 2 cm apart and 3 pCi/mm^2 specific activity. The fourth aggregate on the right top corner is made of non UV-damaged, hence non repairing cells; its image is a simulation of the expected radioactivity background in a "mutant cells" colony.

replication is almost completely blocked by the inhibitor, the radioactive precursor will mainly be utilized by the cells engaged in the repair of the DNA damaged by the UV-treatment.

Fig. 12 is a map, as reconstructed with the MWPC, of four living cells aggregates obtained with this procedure. Their relative distance is 2 cm and the active area is 12 or 19 mm^2. The specific activity of each aggregate, as measured with a liquid scintillator technique, is $\simeq 10$ pCi/mm^2. Fig. 13 is the optical densitogram of a section through the cells shown to the right of Fig. 11. In Fig. 14 a similar map is shown, but the specific activity is now 3 pCi/mm^2. The cells in the right-hand corner of the picture were not exposed to UV light and their image simulates the expected background activity in a non repairing colony.

5. - THE DIGITAL READ-OUT SYSTEM.

The signals from the x and y TAC's are digitized by means of two 12 bit ADCs' and stored in the permanent storage (floppy-disk) of a DEC-MINC 11 minicomputer (Fig. 15). The data are first organized as a 64 x 64 (or 128 x 128) matrix and then analyzed an displayed with an image processing specialized hardware and software.

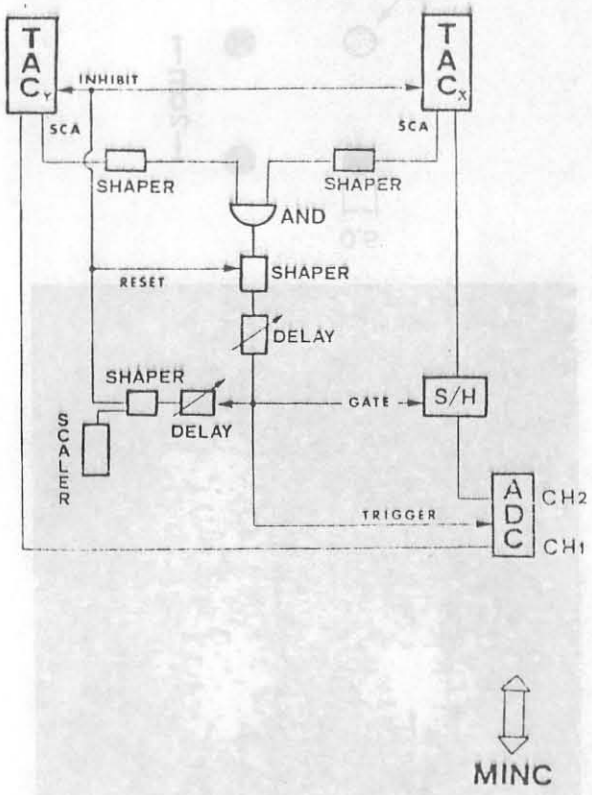

FIG. 15 - The digital read-out system: detailed view.

Computer controlled data acquisition, handling and display have shown significant advantages over the analog one we previously used (oscilloscope coupled Polaroid camera), in terms of:

1) grey (or colour) scaling independently of the film characteristics;
2) possibility of correction for non linearity and non uniformity;
3) processing of images with poor statistics, i. e. improvement of the S/N;
4) image enhancement and pattern recognition;
5) possibility of correction for resolution degradation; i. e. refocussing (deconvolution) techniques;
6) absolute parameters measurement.

In Fig. 16 two ^{14}C individual sources, 2 mm in diameter, 20 mm apart are displayed whithout (left) and with (right) a constant level (background) subtraction. The FWHM of the profiles trough the center of these sources can be estimated $\simeq$ 4.5 mm and $\simeq$4.0 mm respectively. Typi

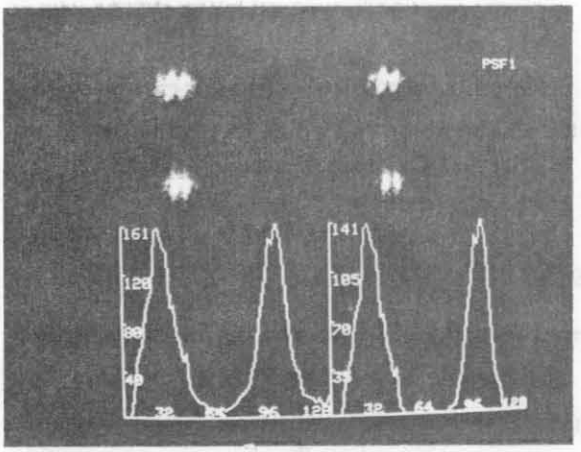

FIG. 16 - Two digitally reconstructed ^{14}C sources, 20 mm apart, 2 mm diameter original (upper left-hand side), background substraction (upper right-hand side) and their relative profiles.

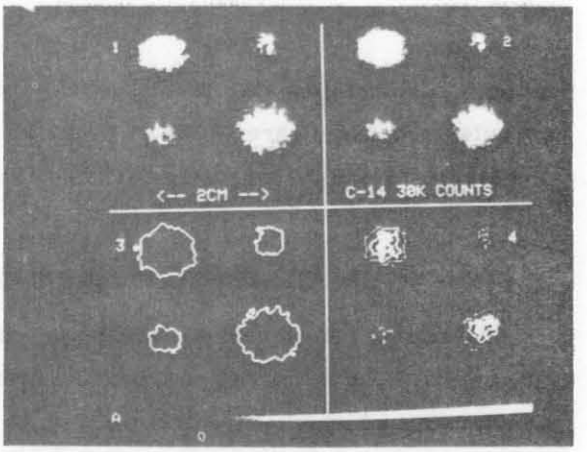

FIG. 17 - Processed maps of four ^{14}C-labelled cells aggregates of different areas (12-19 mm^2) and activity (7-10 pCurie/mm^2) : 1) original, 2) smoothing, 3) Region of interest (ROI).

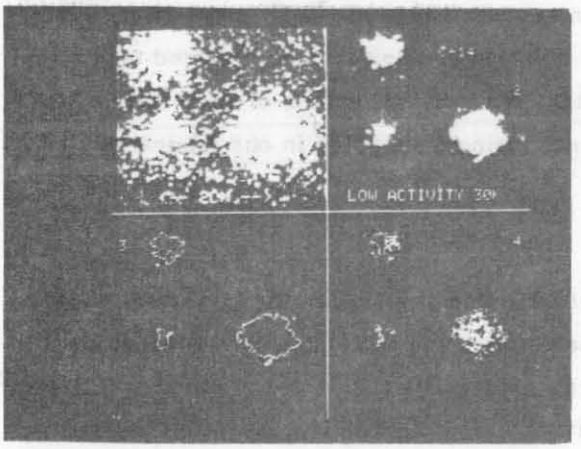

FIG. 18 - Processed maps of three ^{14}C-labelled cell aggregates of different areas (7 12--19 mm^2) and very low activity (≃ 3pCurie/mm^2) : 1) original, 2) smoothing and background subtraction, 3) ROI, 4) isocount lines.

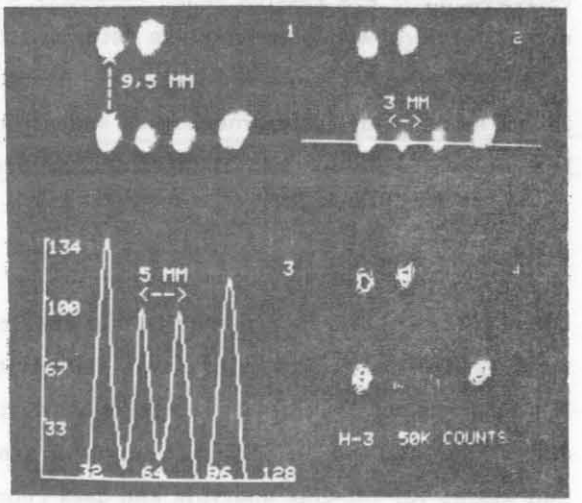

FIG. 19 - Processed maps of six ^{3}H-labelled cellular monolayers. The minimum distance between two layers is 2,5 mm : 1) original, 2) smoothing + background subtraction, 3) a profile trough the line shown in 2, 4) isocount lines.

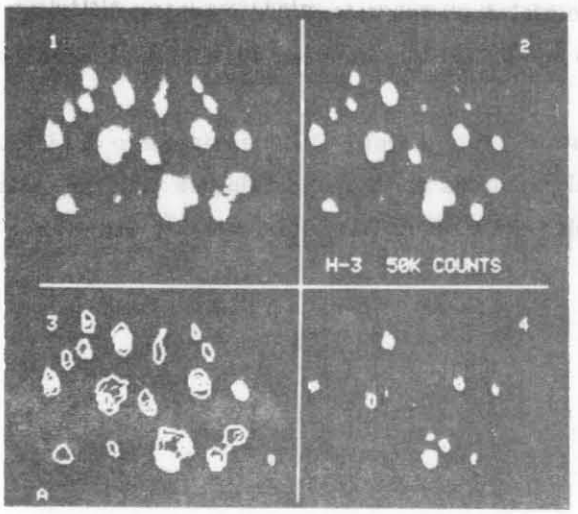

FIG. 20 - Processed maps of several clones of ^{3}H-labelled cells. The mean density is 2 clones/cm^2. 1) original, 2) smoothing + background subtraction, 3) isocount lines, 4) more selective contouring showing the internal structures in some contours.

NOTE : The originals are colour pictures; The passage to black and white print greatly impairs the quality and information density.

cal digital autoradiographs of ^{14}C labelled living cells as obtained with simple and standard computer processing are shown in Figs. 17 and 18. They can be favorable compared with the corresponding analog ones (Figs. 12 and 14).

6. - IMAGING OF ^{3}H-LABELLED LIVING CELLS.

The use of ^{3}H-thymidine labelling greatly increases the specific activity of the colonies and improves the resolving power of the system. The former is increased by more than a factor ten using a higher concentration of quite cheaper ^{3}H-thymidine, while the latter is reduced up to $\simeq$ 1.5 mm (FWHM) because of the very short range of the ^{3}H β^- rays (few millimeters in Argon S. T. P.). Figs. 19 and 20 show reconstructed and processed maps of ^{3}H labelled cellular monolayers and of clones of living cells as obtained directly putting the samples inside the gas volume of the detector. The main problem with ^{3}H-labelling is the necessity of working with a windowless detector. The maximum range of ^{3}H β^- rays (E_{MAX} = = 18 keV) is in fact only $\simeq$ 5 mg/cm^2. A suitable solution can however be realized with a little bit more complicated mechanics and gas tighting. A modified version of our detector allowing the routine use of ^{3}H-labelled samples is now being assembled in our laboratory.

7. - CONCLUSIONS.

We have shown that a MWPC is a very useful detection system for the biological experiment we proposed. Resolving power, linearity, sensitivity are good enough to reconstruct biological maps of ^{14}C-labelled living cells that have a typical specific activity of some pCi/mm^2 and - 1 cm separation. Further improvements are obtained digitalizing the whole system, that allows for off-line analysis and data reduction, and particularly using -labelling.

ACKNOWLEDGEMENTS.

We are truly indebted to C. Cerri for many helpful discussions and for providing us with the preamps. It is a pleasure to thank G. Gennaro and R. Ruberti for their technical support in designing and constructing the chamber.

A particular thanks to A. Abbondandolo (Istituto di Mutagenesi e Differenziamento del CNR di Pisa) for many useful discussions on biological problems and for providing us with the cells samples and to M. Zito (Istituto di Fisiologia Clinica del CNR di Pisa) for valuable assistance during image processing.

REFERENCES.

(1) - J. E. Cleaver, Nature 218, 652 (1968).

(2) - R. Bellazzini, A. Del Guerra, M. M. Massai, M. Ragadini, G. Spandre and G. Tonelli, Nucl. Instr. and Meth. 190, 627 (1981).

(3) - R. Bellazzini, G. Betti, A. Del Guerra, M. M. Massai, M. Ragadini, G. Spandre, G. Tonelli and R. Venturi, Submitted to Nucl. Instr. and Meth.